Portable X-band system for solution state dynamic nuclear polarization

Brandon D. Armstrong [a], Mark D. Lingwood [b], Evan R. McCarney [b,c],
Elliott R. Brown [d], Peter Blümler [e], Songi Han [b,c,*]

[a] Department of Physics, University of California, Santa Barbara, CA 93106, USA
[b] Department of Chemistry and Biochemistry, University of California, Santa Barbara, CA 93106, USA
[c] Materials Research Laboratory, University of California, Santa Barbara, CA 93106, USA
[d] Department of Electrical and Computer Engineering, University of California, Santa Barbara, CA 93106, USA
[e] Research Center Jülich, ICG Phytosphere, 52425 Jülich, Germany

Abstract

This paper concerns instrumental approaches to obtain large dynamic nuclear polarization (DNP) enhancements in a completely portable system. We show that at fields of 0.35 T under ambient conditions and at X-band frequencies, ^{1}H enhancements of >100-fold can be achieved using nitroxide radical systems, which is near the theoretical maximum for ^{1}H polarization using the Overhauser effect at this field. These large enhancements were obtained using a custom built microwave transmitter and a commercial TE_{102} X-band resonant cavity. The custom built microwave transmitter is compact, so when combined with a permanent magnet it is readily transportable. Our commercial X-band resonator was modified to be tunable over a range of ~9.5–10 GHz, giving added versatility to our fixed field portable DNP system. In addition, a field adjustable Halbach permanent magnet has also been employed as another means for matching the electron spin resonance condition. Both portable setups provide large signal enhancements and with improvements in design and engineering, greater than 100-fold ^{1}H enhancements are feasible.
© 2008 Published by Elsevier Inc.

Keywords: Dynamic nuclear polarization; X-Band DNP; Overhauser effect; Portable DNP

1. Introduction

The *in vitro* and *in vivo* analysis of biological samples greatly relies on non-invasive spectroscopic techniques that operate on bulk fluid samples under native biological conditions. Nuclear magnetic resonance (NMR) is, according to these criteria, a superior tool for providing detailed molecular signatures and images utilizing very low-energy radio frequency (RF) irradiation (10–900 MHz) and endogenous probes (e.g. ^{1}H) of the biological sample that cohere sufficiently long to be detected at ambient temperatures. Magnetic resonance imaging (MRI) is capable of producing images of the entire human body by employing the ^{1}H signal of the most abundant molecule in biology, water. However, both NMR and MRI suffer from insufficient sensitivity and signal overlap of the abundant endogenous probes.

Electron spin resonance (ESR), a complementary technique to NMR, utilizes the much stronger magnetic moment of the electron spins for signal (approximately 660 times stronger than proton), but requires the presence of unpaired electrons. For diamagnetic biological samples, this is achieved by attaching stable nitroxide radicals, called spin-labels, to the molecule of interest, which means that no direct signature from the molecule is utilized. Dynamic nuclear polarization (DNP) is a method that transfers part of the orders-of-magnitude larger electron spin polarization of radical species to the nuclear spin polarization, thus greatly amplifying the NMR and MRI signal and increasing the sensitivity and/or contrast. There

are four DNP processes that can transfer polarization from electron to nuclear spins; the Overhauser Effect [1], solid effect [2], thermal mixing [3], and the cross effect or electron–nuclear cross polarization (eNCP) [4]. Our current investigations are on solutions of dissolved molecules and free radicals at low fields (0.35 T) and take advantage of the Overhauser effect, which will therefore be the only method discussed in detail. The thermal mixing and cross effect can be effective at the high magnetic fields required for NMR spectroscopy, and the necessary technology is becoming more advanced because of the method's unique capabilities[5,6] even though complex and expensive instrumentation is required. Overall, DNP amplification techniques are gaining more attention for applications that require enhanced sensitivity and/or information contrast.

The Overhauser effect has found applications in Overhauser enhanced magnetic resonance imaging (OMRI) [7–12], flow imaging by remotely enhanced liquids for imaging contrast (RELIC) [13], or determining local viscosities near a spin-labeled micelle from changes in the Overhauser enhancement (unpublished). The efficiency of the Overhauser effect decreases with the magnetic field [14], but it is still effective at 0.35 T where electron spin resonance occurs at X-band frequencies that are relatively easy to generate, amplify and detect [15].

We report here two advances we recently achieved in producing Overhauser enhanced DNP. Using a custom built X-band microwave transmitter, we have recorded ¹H enhancements of TEMPO/water solutions of 131 ± 6-fold, which is the largest experimentally measured amplification factor at 0.35 T we have seen reported. For these measurements, an electromagnet and Bruker TE_{102} cavity were employed. The other focus is to report on our development of a fully portable DNP polarization system at 0.35 T, composed of a fixed-field or mechanically variable-field Halbach type permanent magnet, a modified Bruker TE_{102} resonant cavity and a custom X-band microwave transmitter. So far, we have achieved ¹H enhancement of -65 ± 9-fold in the portable DNP system based on the fixed field permanent magnet and -80 ± 15-fold using the variable-field Halbach magnet. A portable DNP system can be useful if it is to be used in conjunction with other biomedical instrumentation, at different laboratories, or on time-sensitive or *in vivo* applications. More generally, a portable DNP system can be advantageous when added to portable NMR imaging systems that operate at lower magnetic fields and therefore usually suffer from insufficient polarization and sensitivity.

2. Theory

An in-depth description of the Overhauser effect can be found in several references [1,14,16,17], so only a brief summary relevant for free radicals dissolved in solution and free radicals attached to other molecules dissolved in solution will be provided here. The Overhauser effect is typically described with the four level energy diagram shown

in Fig. 1, where S represents an electron spin and I represents a nuclear spin (often a proton). Through dipolar and/or scalar coupling, the cross relaxation terms w_o and w_2 are non-zero. Thus, creating a non-equilibrium distribution of S spins by saturating the electron spin resonance can lead to enhanced nuclear magnetic resonance signal of the I spins through the cross relaxation transitions. This enhancement, E, is defined as $\langle I_z \rangle / \langle I_o \rangle$, where $\langle I_o \rangle$ is the steady-state equilibrium polarization, and is given by [14]

$$E = 1 - \rho f s \frac{|\gamma_S|}{\gamma_I}, \tag{1}$$

where γ_I and γ_S are the gyromagnetic ratios of the I and S spins, respectively,

$$\rho = \frac{w_2 - w_o}{w_o + 2w_1 + w_2}, \tag{2}$$

$$f = \frac{w_o + 2w_1 + w_2}{w_o + 2w_1 + w_2 + w^o} = \frac{kCT_{10}}{1 + kCT_{10}} = 1 - \frac{T_1}{T_{10}}, \tag{3}$$

and on resonance of the S transition,

$$s = \frac{AP}{1 + BP}. \tag{4}$$

The coupling factor, ρ, expresses the efficiency of dipolar or scalar coupling between the electron and nucleus, can vary between 0.5 for pure dipolar coupling and -1 for pure scalar coupling, and has a strong field dependence [14]. The leakage factor, f, depends on the concentration, C, of the free radical relaxing the nuclei and can be easily determined by measuring the longitudinal relaxation times of the solvent with (T_1) and without (T_{10}) the free radical. As seen in Eq. 3, f approaches 1 in the limit of high radical concentrations, where "high" radical concentration is determined by the relaxivity constant, k, describing how effectively the electron relaxes the nuclear spin compared to the internal nuclear spin relaxation mechanisms. The saturation factor, s, is a function of the applied radiation power driving the electron spin transition, P. Traditionally, the constants A and B are given by $A = \alpha/n$ and $B = \alpha$, where α is a constant dependent on the electron spin relaxation times and radiation source properties, and n is the number of hyperfine lines in the ESR spectrum [18]. However, our findings were that A and B are more generally also functions of the
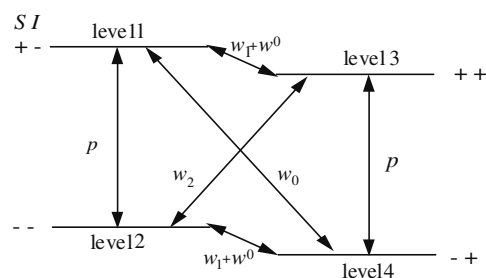

Fig. 1. Four-level energy diagram for the electron–proton coupled 2-spin system. The transitions w_1, w_2, and w_0 represent dipolar and/or scalar induced transitions. The intrinsic electron relaxation rate is p and the intrinsic nuclear spin relaxation rate is given by w^0.

Heisenberg electron spin exchange rate, intrinsic electron spin relaxation rate, and in the case of the commonly used nitroxide radicals, the nitrogen nuclear spin relaxation rate, as quantitatively detailed elsewhere [15]. In the limit of high microwave power P, $s \rightarrow A/B = s_{max}$, which can vary between $1/n$ and 1 depending on the various factors listed above [15]. We use the terminology E_{max} for the DNP enhancement factor (E) in the limit of infinite power. For nitroxide radicals, the Heisenberg spin exchange effect increases s_{max}, and thus the maximum DNP enhancement, to near that of a single-line radical at concentrations around 10 mM. However, Heisenberg spin exchange also broadens the ESR absorption lines [19], so that more microwave power is needed to saturate the electron spin transition at higher radical concentrations in order to obtain the maximum saturation factor, and thus maximum DNP enhancement. Also, at nitroxide concentrations above 10 mM, relaxation measurements show the leakage factor to be near 1, so that from (Eq. 1) $E_{max} \sim 1 - \rho^* 660$ for these large concentrations.

3. Results and discussion

3.1. Characterization of custom microwave source

Here we discuss the power output and sample heating caused by our custom transmitter and amplifier, while the specifics of the custom X-band microwave amplifier design are discussed in the experimental section. The output power was measured using an EIP 548A frequency counter equipped with a power meter. The maximum output power was measured to be about 23 W. Two 9 dB step attenuators in series allow the output power to be varied from 23 W (0 dB) to $\sim$370 mW (18 dB). However, this is the power being delivered from the transmitter to an SMA-to-waveguide connector (where the waveguide then couples to the TE_{102} cavity) and not to the sample. To determine the power delivered to the sample, DNP enhancements were measured using a commercial microwave bridge from Bruker Biospin (ER 041 MR; Gunn diode source) designed for ESR measurements and controlled by an EMX spectrometer which displays the power reaching the resonant cavity under output-leveled and matched condition. These enhancements were then compared to enhancements obtained with our custom source at a series of lower output power settings, which allowed us to determine the actual power reaching the sample within error. For example, using commercial ESR equipment an enhancement of −23.5 was measured for a sample of 4-oxo-TEMPO dissolved in water with 126.9 mW of power. Using the same sample with our custom source, an enhancement of −23.4 was measured with 17 dB attenuation (corresponding to $\sim$460 mW ouput power), providing a reference for how much power was reaching the sample. Thus only about 1/4 of the input power was found to actually reach the sample. The small amount of power reaching the sample is largely due to the cavity being used unmatched

because the plastic screw the iris is attached to was damaged by the high power microwaves, so it was removed when performing DNP experiments with our custom source. To account for inaccuracies in the attenuation control in our custom source we used directional couplers to monitor both the forward and reflected power. Through the entire range, the percent of measured reflected power was a constant, so we are able to conclude a 1 dB increase in output power corresponds to 1 dB increase in power reaching the sample.

With such high power microwave radiation reaching the cavity, sample heating can be a significant problem. To limit the amount of heating, cooling air was flowed over the sample. This was found to significantly reduce the amount of sample heating so that little heating was observed with $\sim$2 W reaching the sample. To quantify the heating effect, the bottom of a pasteur pipette was sealed and the pipette was filled with water. A thermocouple was placed inside, but kept just out of the microwave region. The inner diameter of the pipette inside the cavity was 1 mm, while 0.7 mm is the inner diameter of all sample tubes usually used for DNP measurements in this paper. Fig. 2 shows the temperature measured at different powers with and without the use of cooling air. It can be seen that the use of cooling air greatly reduces sample heating. However, as will be discussed below, if sample heating is not a concern, larger signal enhancements compared to room temperature measurements can be measured at elevated temperatures.

3.2. Enhancements using custom microwave source

Using our custom-built microwave amplifier, commercial TE_{102} resonant cavity, and an electromagnet, we believe we have achieved the largest [1]H Overhauser enhancements reported at 0.35 T. Our largest measured enhancement of −130-fold was obtained using a sample of ^{15}N substituted 15 mM 4-oxo-TEMPO dissolved in water using the maximum power of our custom microwave
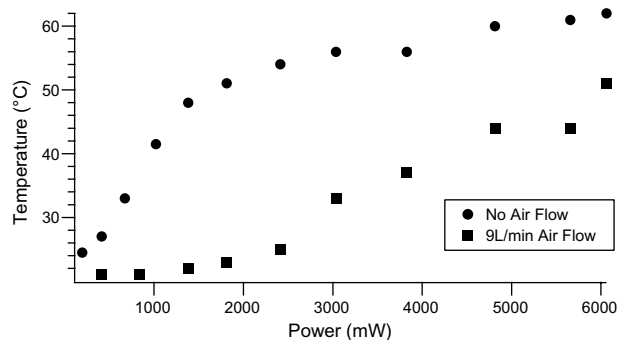

Fig. 2. The sample temperature measured as a function of microwave power reaching the sample with (squares) and without (circles) cooling air. The use of cooling air greatly reduces sample heating such that at 2.4 W of microwave power the sample temperature was only 25 °C compared to 54 °C without the use of cooling air.

source and no cooling air. Table 1 shows a list of measured DNP enhancements for several different samples, where cooling air was used for all measurements (except for the just mentioned sample), and the microwave power was attenuated 5 dB before coupling to the waveguide so that the power at the sample was ∼2.4 W. At this power, with the use of cooling air, there is minimal heating as seen in Fig. 2. Previously for ^{15}N and ^{14}N 15 mM 4-oxo-TEMPO samples dissolved in water, we reported maximum possible enhancement factors (E_{max}) of −108 ± 5 and −95 ± 4, respectively [15]. Thus, the measured enhancements listed in Table 1 appear to have already reached these maximum values. However, when extrapolating the enhancement vs. power curves shown in Fig. 3 to infinite power using Eq. 1, a maximum enhancement factor of ∼−130 for all samples is predicted. As this is true for both 15 and 100 mM radical concentrations, the maximum saturation factor and leakage factors must be nearly equal, i.e. nearly 1. A maximum enhancement of −130 implies a slightly larger coupling factor of $\rho \sim 0.2$ for nitroxide radicals as opposed to our previously reported value of $\rho = 0.18$, which number was obtained through measurements using only a maximum of 200 mW microwave power [15].

Another interesting conclusion to draw from the observation that both the ^{15}N substituted nitroxide radicals and the ^{14}N nitroxide radicals give comparable enhancement factors and extrapolate to nearly equal values at infinite power is that Heisenberg exchange is effectively mixing the hyperfine electron spin states at 15 mM radical concentration. This implies the maximum saturation factor for all the listed radicals is near 1 [15,20]. Thus, at high concentrations and sufficient microwave power, there is no advantage to using a more expensive ^{15}N substituted radical. However, both Table 1 and Fig. 3 show that for a given lower power output, the ^{15}N nitroxide radicals give larger enhancements. This can be explained through the ESR
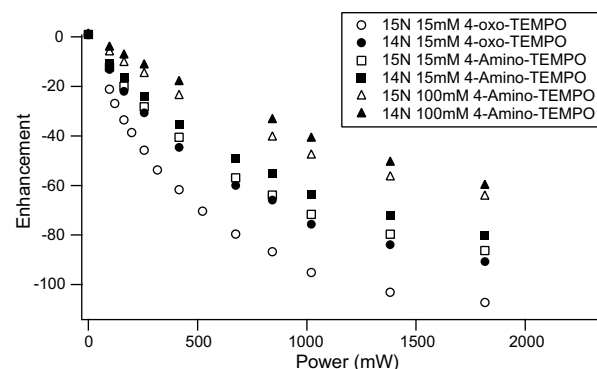

Fig. 3. The Enhancement vs. Power curves for the six different aqueous nitroxide samples listed in Table 1 with the use of cooling air. Samples with the narrowest ESR lines achieve larger enhancements at a given power, but all samples extrapolate to an enhancement of ∼−130 at infinite power. The difference in observed enhancements between ^{15}N substituted and ^{14}N natural abundance nitroxides is small indicating Heisenberg Exchange is effectively mixing the electron spin hyperfine states.

linewidth of the different samples listed in Table 1. Even though the maximum possible enhancement factors for each sample are nearly equal, the measured enhancements precisely follow the ESR linewidths, with the narrowest line giving the largest enhancements.

An enhancement factor of −130 was measured for 15 mM ^{15}N 4-oxo-TEMPO under conditions where significant heating is expected (6 W of power, no cooling air), while an enhancement of only −112 ± 4 was measured under conditions when sample heating should be minimal (2.4 W of power, 9 L/min cooling air; Fig. 2. This can be explained by looking at the expected changes in the coupling factor and thermal polarization with increasing temperature. A rise in temperature from 20 to 60 °C (Fig. 2) corresponds to a loss in thermal polarization of ∼17%. However, in both the rotational and translational DNP models, the coupling factor has a strong dependence on the solvent viscosity [21], which decreases by 53% for the same temperature change [22]. Using only the translational model [14], and assuming a coupling factor of 0.2 at room temperature, a 53% decrease in viscosity results in a 50% increase in the coupling factor, thus from 0.20 to 0.30. Hence, even though an increase in temperature leads to significant decrease of thermal polarization, it still can result in a much larger signal enhancement compared to the unenhanced signal at room temperature.

3.3. Portable DNP

Our custom microwave source and amplifier provides the largest power output among sources that are not based on traveling wave tube amplifiers, while ensuring high frequency and phase stability as well as great frequency tunability, given by the characteristics of a phase-locked YIG (yttrium–iron–garnet) synthesizer (Microlambda Wireless, CA). The key components are based on solid state devices, and are thus very compact. The YIG synthe-

Table 1
The measured enhancements for six different aqueous solution samples using our custom microwave source together with the commercial resonant cavity

Radical	Conc (mM)	ESR ΔB_{pp} (gauss)	Meas. E	E_{max}	Cooling air
15N 4-oxo[a]	15	1.15	−131 ± 6	——	No
15N 4-oxo	15	1.15	−112 ± 4	−136 ± 8	Yes
14N 4-oxo	15	1.57	−98 ± 3	−131 ± 8	Yes
15N 4-amino	15	1.6	−94 ± 4	−127 ± 8	Yes
14N 4-amino	15	2.33	−88 ± 3	−126 ± 6	Yes
15N 4-amino	100	7.35	−72 ± 3	−121 ± 9	Yes
14N 4-amino	100	7.72	−71 ± 3	−124 ± 10	Yes

The ESR derivative linewidth (ΔB_{pp}) of a sample is a good measure for the ease of saturation of a sample. Narrower lines are easier to saturate, and thus reach higher enhancements for a given output power. For all samples, the power was ∼2.4 W and cooling air was used except[a]; this sample was measured at maximum output power without cooling air. E_{max} was determined by extrapolation of the Enhancement vs. Power curves in Fig. 3 to infinite power using Eq. 1.

sizer, solid state power amplifiers, 10 MHz reference, and power supply (each described in detail in the experimental section) easily fit on a tabletop or cart (Fig. 4). The large electromagnet was replaced by two different types of permanent magnets. One is a fixed field, commercially available, permanent magnet with a 35 mm gap, where the B_0 field is normal to the pole surface (Fig. 4). The second is a field adjustable Halbach magnet [23–25] available to us only recently and not yet commercially available (Fig. 5). The Halbach magnet has a cylindrical bore with 100 mm inner diameter, with the B_0 field perpendicular to the cylinder axis. Both magnets have sufficiently large gaps, so that the commercial Bruker TE_{102} resonant cavity fits inside.

It is important to have the ability to either tune the microwave frequency or to adjust the magnetic field in order to precisely match the electron spin resonance condition. As the frequency bandwidth of X-band ESR cavities is usually very narrow, the cavity has to be made frequency-tunable for the former scenario, while the latter case is necessary for a fixed-frequency cavity. These methods have advantages over adding resistive coils to a fixed field permanent magnet in that another power supply is not necessary, and the field of the permanent magnet is not affected by the heating of the resistive coils.

Our commercial TE_{102} resonant cavity was modified so that the resonant frequency could be made tunable for its use in the fixed field permanent magnet. This was realized by making the wall opposite along which the microwave is coupled in via the wave guide (the long axis of the reso-

nator) adjustable with a copper plate attached to a non-magnetic screw. A non-magnetic spring was placed between the moveable wall and a fixed plate attached to the cavity. By turning the screw, the copper plate can move further in or out of the resonator, thus varying the length of the cavity and resonant frequency. To test the range over which significant DNP enhancements could be measured in the modified cavity, it was placed in the electromagnet with a sample of 15 mM ^{15}N 4-oxo-TEMPO, so that the field could be adjusted to match the ESR condition. The frequency at which the cavity was resonating was monitored using the Bruker EMX spectrometer and EIP frequency counter. Our custom microwave source was then coupled to the cavity, set to the resonant frequency of the cavity, and the DNP enhancement measured. Enhancements were measured over a range of 9902.5 to 9528.5 MHz, corresponding to a change in field from 3522 to 3389 gauss, which were the mechanical limits of our modified cavity. By changing the length of the cavity, the location in the cavity at which the maximum B_{1e} field is transmitted changes, which results in reduction of DNP enhancements, as the sample is in a fixed position inside the cavity. This effect can perhaps be seen in Fig. 6 which shows the measured DNP enhancement factors versus frequency. There is a decrease in enhancement at the highest frequencies, which is likely due the maximum B_{1e} location moving further away from the center when changing the length of the cavity, thus from the sample. At the lowest frequency of 9528.5 MHz, there is a sudden and large drop in enhance-
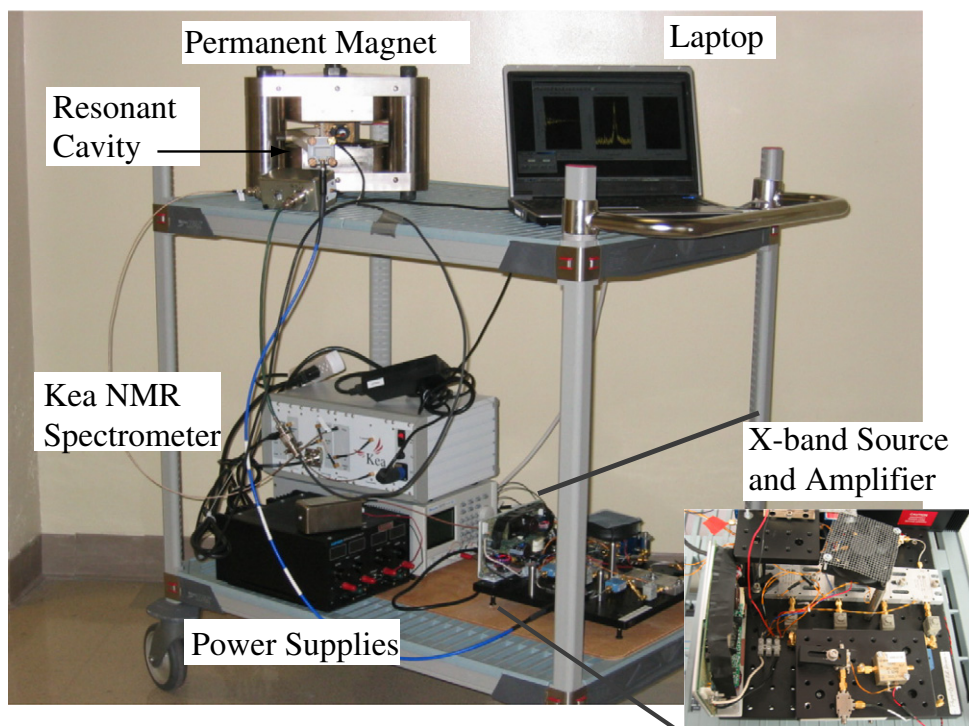

Fig. 4. The complete portable setup on a cart ready for transportation or use. The power supplies, custom microwave source, and *Kea* NMR spectrometer are set on the bottom of the cart and the permanent magnet with the resonant cavity on top. A laptop controls the frequency output of the YIG and the NMR spectrometer.
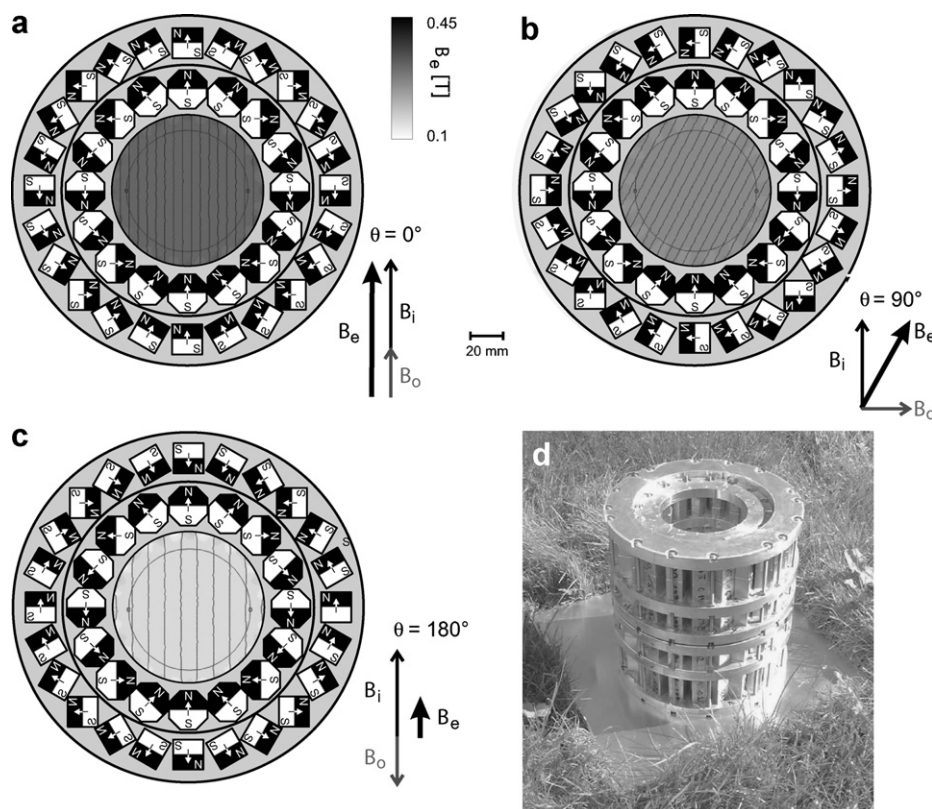
Fig. 5. Function and design of the Halbach permanent magnet for DNP. (a–c) Rotation of the nested rings. (a) Both rings parallel ($\theta = 0°$), (b) perpendicular ($\theta = 90°$) and (c) antiparallel ($\theta = 180°$). The vectors illustrate the vector addition of the fields. The center of the inner ring shows a simulation of the resulting field with field lines and gray shaded to illustrate direction and strength of the resulting field. (d) photograph of the magnet.
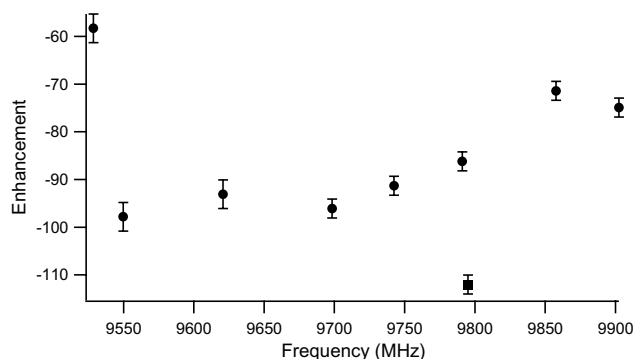

Fig. 6. The Enhancement vs. Frequency for our adjustable cavity with a sample of 4-oxo-TEMPO in solution in an electromagnet where the field can be precisely adjusted to match the electron spin resonance condition. The square point represents the enhancement in the unmodified commercial cavity. The frequency at which the cavity resonates was determined using a Bruker EMX spectrometer and EIP frequency counter.

ment, likely because reaching the mechanical limit caused poor alignment of the adjustable wall. Still, over a large frequency range of nearly 200 MHz, greater than −90-fold enhancements were measured with the maximum enhancement being −98-fold. An enhancement of −112 was measured for the same sample in the unmodified commercial cavity. We attribute this small decrease due to a somewhat lower Q in our modified cavity of ~1400 (with coil and

sample loaded), while the commercial cavity has a measured Q of ~2200 and thus more power reaching the sample. While empty, the commercial cavity has a $Q \sim 3200$ compared to 2200 of the modified cavity. There was no noticeable difference in Q values of the cavity with or without the sample inserted into the NMR probe. This experiment shows we are able to reach a wide and useful tuning range by a small modification of the commercial Bruker TE_{102} cavity. This modified cavity can be readily employed with a fixed-field magnet and tunable microwave source to perform DNP experiments.

We placed the modified cavity inside our portable, fixed-field, permanent magnet (Aster Enterprises Inc.,MA). The entire DNP setup is readily portable (Fig. 4) and has been transported to different buildings on campus and used for demonstration purposes. The electron resonant frequency is determined by first measuring the ^{1}H frequency, and then setting the YIG source to the corresponding calculated ESR frequency. To optimize the DNP efficiency, the length of the cavity was adjusted while the proton enhancement was monitored. So far, the maximum measured enhancement in this portable DNP setup, under conditions where little sample heating occurs with a 15 mM, ^{15}N 4-oxo-TEMPO aqueous solution sample, was $−65 \pm 9$. This is about 25% less than what has been measured in the electromagnet with the modified cavity at the same field (−86; Fig. 6), and about 40% less than measured with the unmod-

ified cavity in the electromagnet. We attribute this decrease to the difficulty in tuning the cavity to precisely meet ESR condition with sufficiently high accuracy. With increased microwave power and sample heating, an enhancement of -92 ± 11 was measured. Further design optimizations, such as decreasing the amount of movement of the movable wall of the cavity per turn of the screw to allow for finer adjustments should greatly improve these results.

Alternatively, we used the commercial resonator inside a field adjustable Halbach magnet. As before, the frequency at which the cavity resonates was determined using the Bruker EMX spectrometer and EIP frequency counter. The resonant frequency of the cavity depends on the NMR probe and sample holder being incorporated into its core, but if these are not altered the frequency is precisely reproducible. Thus, once adjusted and optimized, the EMX spectrometer and frequency counter are not necessary parts of the equipment that needs to be transported with the portable setup. An SMA to waveguide adapter was attached directly to the cavity as it would not fit into the magnet when coupled via the waveguide. This setup barely fit into the 100 mm bore of the Halbach magnet and the sample was no longer in the center of the magnet. In principle the magnet could be made with a larger bore and/or the cavity made smaller so it fits more easily inside the bore, which then allows the sample to be positioned at the center. Both of these adjustments are being made for future experiments. The magnetic field was adjusted to match the ESR condition of a ^{15}N 4-oxo-TEMPO sample in aqueous solution determined by the frequency at which the cavity resonates. A ^{1}H enhancement was measured of -80 ± 15 under conditions where no sample heating is expected. This is lower than the -112 measured in the electromagnet, which is due to the difficulty of saturating inhomogeneously broadened ESR lines caused by spatial field distributions across the volume of the sample that is not centered at the field.

4. Conclusion

X-band is the most commonly used frequency band for ESR studies. As ESR and DNP analysis of solution-state samples both critically depend on the dynamics of the radical or spin label, DNP at X-band together with ESR experiments can provide valuable information about the local environment of the spin label as well as dynamics of the labeled molecule itself. For experiments where large signal enhancements are preferred or required, a compact custom microwave transmitter device, composed of readily available solid state components, can be built that is capable of reaching high saturation of the homogeneously and/or exchange broadened ESR lines of nitroxide radicals. The largest reported ^{1}H enhancements at 0.35 T using nitroxide radicals dissolved in water of up to -130-fold with maximum power and sample heating, and -112-fold with lower power and no sample heating have been measured when

using the custom transmitter along with a commercial electromagnet and resonant cavity.

Our goal to build a portable and versatile DNP polarizer has been achieved with ^{1}H enhancements of -65 using a tunable TE_{102} resonant cavity and fixed field permanent magnet. The same custom cavity provided greater than -90-fold enhancement when used with a Bruker EMX spectrometer and electromagnet that can accurately adjust to the resonance condition. Using the field-adjustable Halbach magnet as an alternative portable permanent magnet we have achieved -80-fold enhancement with the commercial TE_{102} resonator. This characterization shows us that we have a fully portable DNP polarizer with good performance. Experiments performed in a commercial electromagnet and resonant cavity show that larger enhancements are possible in our portable setup and that optimal efficiency is within reach with further improvements in cavity engineering and magnet design. As portable NMR is an emerging field, the ability to add DNP capabilities to these experiments may be of great interest.

These experiments were made possible by a compact, custom built, microwave driver and amplifier which is capable of delivering continuous wave microwave irradiation with high power up to 23 W, frequency tunability between 8 and 10 GHz, and frequency instability of less than 100 Hz. The use of cooling air greatly reduces sample heating so that little temperature rise was observed when 2 W of power reaches the sample.

5. Experimental

5.1. Sample preparation

The free radicals 4-oxo-2,2,6,6-tetramethyl-1-piperidinyloxy (4-oxo-TEMPO) and 4-amino-2,2,6,6-tetramethyl-1-piperidinyloxy (4-amino-TEMPO) were purchased from Sigma–Aldrich. Isotope enriched ^{15}N labeled 4-oxo-TEMPO was purchased from Cambridge Isotope Laboratories. ^{15}N labeled ammonia and D_6-acetone were also purchased from Cambridge Isotope Laboratories and used to synthesize ^{15}N labeled 4-amino-TEMPO following published procedures [26]. 4-Amino-Tempo was dissolved directly into de-ionized water while 4-oxo-TEMPO was initially dissolved at a high concentration into DMSO and then diluted into de-ionized water, the final solution containing no more than 5% DMSO by volume. The samples were not degassed. Volumes of approximately 5 μL were loaded into 0.7 mm inner diameter silica capillaries (Polymicro Technologies 2000029) and sealed with beeswax and used for both ESR and NMR measurements.

5.2. ESR and DNP measurements in the electromagnet and portable permanent magnets

ESR experiments were performed at 0.35 T in an electromagnet (field adjustable between 0 and 1.5 T) using a Bruker rectangular resonant cavity operating at 9.8 GHz

in TE_{102} mode and a Bruker EMX spectrometer. A home built double U-coil NMR probe operating at 14.85 MHz was inserted into the microwave cavity under tuned and matched conditions. The NMR experiments were carried out with a Bruker Avance 300 spectrometer as well as an inexpensive and portable *Kea* NMR spectrometer (Magritek Limited, Wellington, New Zealand). DNP experiments were preformed while continuously irradiating the sample with on-resonant (with respect to one of the ESR lines of the nitroxide free radicals) 9.8 GHz microwave irradiation using our custom built microwave driver and amplifier. The frequency source is a phase-locked YIG synthesizer (Microlambda Wireless MLSL-1178) with 27.5 mW output, tunable between 8 and 10 GHz and a frequency accuracy of 100 Hz. The microwave output is sent through two step attenuators (Narda 4741), split with Wilkinson power dividers (Minicircuits ZX10-2-126), directed through four solid state power amplifiers (Advanced Microwave, Inc. PA2803-24) in parallel, protected against reflected power using coaxial isolators with at least 25 dB protection (UTE Microwave Inc. CT-5157-OT), recombined again with a Wilkinson power combiner (MIDISCO MDC2227), and directed into an SMA output with a measure output power of 23 W. A circuit diagram of this transmission device is shown in Fig. 7. The YIG oscillator requires a 10 MHz reference frequency input along with two voltage sources (5 V, 0 A and 15 V, 0.34 A) and a computer for adjusting the frequency via a parallel interface with the supplied program (Microlambda Wireless). For these purposes, we employed an Instek PST-3201 triple output power supply and a Stanford Research Systems SC-10 as a 10 MHz reference source. A SMA to wave guide connector (RF-Lambda RFWA90A, VSWR of 1.20:1 max) is used to couple the microwave output to the Bruker TE_{102} cavity. The precise frequency to set the YIG synthesizer can be found by either monitoring the DNP enhancement while adjusting the frequency or by monitoring the frequency at which the TE_{102} cavity resonates when coupled to the Bruker Bridge (ER 041 MR; a Gunn diode source) using a frequency counter (EIP 548 A). This resonance frequency is accurately reproducible

when using the same sample holder and NMR coil, but can vary significantly if either of these conditions is changed. For experiments using the portable DNP setup with a fixed field magnet, a 0.3487 T (at 22.5 °C with temperature variance of ∼0.025%/°C) permanent magnet was purchased from Aster Enterprises, Inc. This magnet is relatively small in size and transportable (∼68 kg), and has a large opening (35 mm gap) to comfortably place the X-band microwave equipment.

For the portable DNP setup with a variable magnetic field, the custom built permanent magnet consists of two Halbach dipoles [23] realized by two nested MANDHALA rings [24] which can be turned relative to each other in order to change the resulting magnetic field manually [25]. The inner ring (ID 100 mm, OD 156 mm) is a stack of 8 layers each made from 16 octagonal permanent magnets (dimensions $24 \times 24 \times 22.2$ mm) while the outer ring (ID 158 mm, OD 224 mm) consists of 6 layers of 24 quadratic permanent magnets (dimensions $18.6 \times 18.6 \times 32.1$ mm). The principal design is shown in Fig. 5. All layers in both rings have individual distances optimized for maximal homogeneity using BEM software (AMPERES, Integrated Engineering Software, Winnipeg, Canada). Each layer consists of an aluminum support with sockets to house the FeNdB magnets (Magnetic Component Engineering, Luton, UK) with a maximum energy product of 383.6 kJ/m^3 and a remanence of $B_r = 1.408$ T. Free rotation of the rings is assured by a ball-bearing at each end. The final magnet has a height of 230 mm of and a weight of ca. 32 kg. As shown in Fig. 5, the resulting effective magnetic field, B_e, is the vector sum of the fields of the inner ring, B_i, and the outer ring, B_o. If the two rings are oriented at an angle, θ, the field is:

$$B_e = \sqrt{B_i^2 + B_0^2 + 2B_iB_0\cos\theta} \qquad (5)$$

With $B_i \approx 0.3$ T and $B_o \approx 0.15$ T the field can be varied from ca. 0.15 T at $\theta = 180°$ to ca. 0.45 T at $\theta = 0°$. For X-band DNP experiments $B_e \sim 0.35$ T at an angle of $\theta = 84°$. The homogeneity in the center of the magnet was determined by NMR to be better than 20 ppm over 5 mm DSV at this field. The DNP measurement was carried out 20 mm off center with a field-homogeneity of 400 ppm.
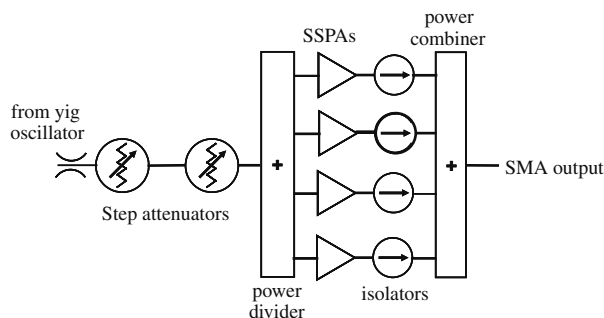
Fig. 7. Circuit diagram of the custom X-band amplifier. The output of the YIG synthesizer source is sent through two step attenuators (0–9 dB each) which are used to vary the power. The power is then divided and sent through four amplifiers (SSPAs) in parallel. Isolators protect the amplifiers from reflected power. The power is then combined and sent through an SMA output to be coupled to the load.

References

[1] A.W. Overhauser, Polarization of Nuclei in Metals, Phys. Rev. 92 (1953) 411–415.

[2] A. Abragam, M. Borghini, Dynamic polarization of nuclear targets, Progr. Low Temp. Phys. 4 (1964) 384–449.

[3] R.A. Wind, M.J. Duijvestijn, C. van der Lugt, A. Manenschijn, J. Vriend, Applications of dynamic nuclear polarization in 13C NMR in solids, Prog. Nucl. Mag. Res. Spectrosc. 17 (1985) 33–67.

[4] V. Weis, R.G. Griffin, electron–nuclear cross polarization, Solid State Nucl. Magn. Reson. 29 (2006) 66–78.

[5] V.S. Bajaj, C.T. Farrar, I. Mastovsky, J. Vieregg, J. Bryant, B. Elena, K.E. Kreischer, R.J. Temkin, R.G. Griffin, Dynamic nuclear polarization at 9T using a novel 250 GHz gyrotron microwave source, J. Magn. Reson. 160 (2003) 85–90.

[6] J. Wolber, F. Ellner, B. Fridlund, A. Gram, H. Johannesson, G. Hansson, L.H. Hansson, M.H. Lerche, S. Mansson, R. Servin, M. Thaning, K. Golman, J.H. Ardenkjaer-Larsen, Generating highly polarized nuclear spins in solution using dynamic nuclear polarization, Nucl. Instrum. Methods Phys. Res. Sect. A-Accelerators Spectrometers Detectors and Associated Equipment 526 (2004) 173–181.

[7] M. Alecci, I. Seimenis, S.J. McCallum, D.J. Lurie, M.A. Foster, Nitroxide free radical clearance in the live rat monitored by radio-frequency CW-EPR and PEDRI, Phys. Med. Biol. 43 (1998) 1899–1905.

[8] W. Barros, M. Engelsberg, Enhanced Overhauser contrast in proton–electron double-resonance imaging of the formation of an alginate hydrogel, J. Magn. Reson. 184 (2007) 101–107.

[9] K. Golman, I. Leunbach, J. Stefan Petersson, D. Holz, J. Overweg, Overhauser-enhanced MRI, Acad. Radiol. 9 (2002) S104–S108.

[10] M.C. Krishna, S. English, K. Yamada, J. Yoo, R. Murugesan, N. Devasahayam, J.A. Cook, K. Golman, J.H. Ardenkjaer-Larsen, S. Subramanian, J.B. Mitchell, Overhauser enhanced magnetic resonance imaging for tumor oximetry: coregistration of tumor anatomy and tissue oxygen concentration, Proc. Natl. Acad. Sci. USA 99 (2002) 2216–2221.

[11] J. Lurie David, H. Li, S. Petryakov, L. Zweier Jay, Development of a PEDRI free-radical imager using a 0.38 T clinical MRI system, Magn. Reson. Med. 47 (2002) 181–186.

[12] D.J. Lurie, G.R. Davies, M.A. Foster, J.M.S. Hutchison, Field-cycled PEDRI imaging of free radicals with detection at 450 mT, Magn. Reson. Imaging 23 (2005) 175–181.

[13] E.R. McCarney, B.D. Armstrong, M.D. Lingwood, S. Han, Hyperpolarized water as an authentic magnetic resonance imaging contrast agent, Proc.Natl. Acad. Sci. USA 104 (2007) 1754–1759.

[14] K.H. Hausser, D. Stehlik, Dynamic nuclear polarization in liquids, Adv. Magn. Reson. 3 (1968) 79–139.

[15] B.D. Armstrong, S. Han, A new model for Overhauser enhanced nuclear magnetic resonance using nitroxide radicals, J. Chem. Phys. 127 (2007) 104508–104510.

[16] A. Abragam, The Principles of Nuclear Magnetism, Clarendon Press, Oxford, England, 1961, pp. 289-305..

[17] I. Solomon, Relaxation Processes in a System of 2 Spins, Phys. Rev. 99 (1955) 559–565.

[18] I. Nicholson, D.J. Lurie, F.J.L. Robb, The application of proton–electron double-resonance imaging techniques to proton mobility studies, J. Magn. Reson. B 104 (1994) 250–255.

[19] J.A. Weil, J.R. Bolton, J.E. Wertz, Electron Paramagnetic Resonance: Elementary Theory and Practical Applications, Wiley, New York, 1994, pp. 309–311..

[20] R.D. Bates, W.S. Drozdoski, Use of nitroxide spin labels in studies of solvent–solute interactions, J. Chem. Phys. 67 (1977) 4038–4044.

[21] W. Muller-Warmuth, K. Meise-Gresch, Molecular motions and interactions as studied by dynamic nuclear polarization (DNP) in free radical solutions, Adv. Magn. Reson. 11 (1983) 1–45.

[22] W.E. Forsythe, Smithsonian Physical Tables, 9th revised ed., Knovel, 1954/2003, 319 pp.

[23] K. Halbach, Strong rare earth cobalt quadrupoles, IEEE Trans. Nucl. Sci. NS 26 (3) (1979) 3882–3884.

[24] H. Raich, P. Blümler, Design and construction of a dipolar Halbach array with an homogeneous field from identical bar-magnets—NMR-Mandhalas, Conc. Magn. Reson. B: Magn. Reson. Eng. 23B (1) (2004) 16–25.

[25] T.R. Ni Mhiochain, J.M.D. Coey, D.L. Weaire, S.M. McMurry, Torque in Nested Halbach Cylinders, IEEE Trans. Magn. 35 (5) (1999) 3968–3970.

[26] E.R. McCarney, S. Han, Spin-labeled gel for the production of radical-free dynamic nuclear polarization enhanced molecules for NMR spectroscopy imaging, J. Magn. Reson. (2008), doi:10.1016/j.jmr.2007.11.013.